Altitudinal and Temporal Variations of Near-Surface Air Temperature Lapse Rate on the Northern Slope of the Tianshan Mountains

YONGKE YANG,[a,b] PENGFENG XIAO,[c] XUELIANG ZHANG,[c] XUEZHI FENG,[c] JIANGENG WANG,[d] NAN YE,[e] ZUO WANG,[f] GUANGJUN HE,[g] AND LIZAO YE[c]

[a] *Department of Geographic Information Science, Central South University of Forestry and Technology, Changsha, China*
[b] *Key Laboratory for Digital Dongting Lake of Hunan Province, Changsha, China*
[c] *School of Geography and Ocean Science, Nanjing University, Nanjing, China*
[d] *School of Atmospheric Science, Nanjing University of Information Science and Technology, Nanjing, China*
[e] *Department of Civil Engineering, Monash University, Melbourne, Victoria, Australia*
[f] *School of Geography and Tourism, Anhui Normal University, Wuhu, China*
[g] *State Key Laboratory of Space-Ground Integrated Information Technology, Beijing Institute of Satellite Information Engineering, Beijing, China*

(Manuscript received 24 September 2021, in final form 27 September 2022)

ABSTRACT: Near-surface air temperature lapse rate (NSATLR) is vital for hydrological simulation and mountain climate research in snowmelt-dominated regions. In this study, NSATLRs of two vertical zones (i.e., mountain grassland–coniferous forest belt and alpine meadow belt) of the Manasi River basin on the northern slope of the Tianshan Mountains were calculated using the near-surface air temperature data from 18 observation stations. Furthermore, temporal variations of NSATLRs of these two vertical zones at seasonal, monthly, and daily scales were analyzed, combined with altitudinal differences of local environments. The results show that the temporal variations of NSATLRs are different between these two vertical zones. The steepest monthly NSATLR occurs in July in the mountain grassland–coniferous forest belt and in April in the alpine meadow belt. In spring, summer, and autumn, the hourly NSATLRs in the mountain grassland–coniferous forest belt generally steepen with increasing solar radiation and vice versa, contrary to those in the alpine meadow belt. During winter, the hourly NSATLRs on sunny days are overall positive at night but negative during the day in the mountain grassland–coniferous forest belt. The findings of this study indicate that it is necessary to divide mountains with similar local environments to the study area into different vertical zones to accurately estimate NSATLR, and the use of a fixed NSATLR for different months and vertical zones is not suitable for snowmelt runoff modeling in snow-dominated regions such as the northern slope of the Tianshan Mountains.

SIGNIFICANCE STATEMENT: This study aims to investigate the altitudinal and temporal variations of near-surface air temperature lapse rate (NSATLR) on the northern slope of the Tianshan Mountains and how mountain environments affect NSATLR. This is important because altitudinal differences of mountain environments lead to different NSATLRs, and these altitudinal variations on the northern slope of the Tianshan Mountains are different from those on the Alps at the same latitude. Our results explain how altitudinal differences of mountain environments affect NSATLRs; hence, using a fixed NSATLR for different months and vertical zones is inappropriate, and estimating NSATLRs for different vertical zones is necessary.

KEYWORDS: Climate; Temperature; Mountain meteorology

1. Introduction

The near-surface air temperature (NSAT) is an important attribute of mountain climate, and a key factor affecting the snowmelt process (Aizen et al. 1997; Barnett et al. 2005; Immerzeel et al. 2010; Oerlemans 2005; Sorg et al. 2012). However, limited by the irregular and sparse distribution of observation stations in mountain areas, it is difficult to obtain spatially continuous near-surface air temperature data accurately from the limited in situ observation data (Minder et al. 2010).

The near-surface air temperature lapse rate (NSATLR) is a classical index that describes the altitudinal variation in NSAT (Dodson and Marks 1997; Gardner et al. 2009). It is also a key parameter of the snowmelt runoff model, which is sensitive to the value of NSATLR (Abudu et al. 2016). The commonly used value of NSATLR (−0.65°C per 100 m) is the average of various global environments (Barry 1992; Dodson and Marks 1997). However, the spatial variation of NSATLR is apparent. For example, the average yearly NSATLR in different regions of the Alps varies from −0.80 to −0.39°C per 100 m (Rolland 2003). Thus, using a fixed value in regions with different environments is problematic (Gardner and Sharp 2017).

Many studies have investigated the temporal variation of NSATLR in alpine regions (such as the Alps, Rocky Mountains, Himalayas, and Tianshan Mountains), and the impacts of solar radiation, air humidity, and synoptic events on NSATLR

Supplemental information related to this paper is available at the Journals Online website: https://doi.org/10.1175/JAMC-D-21-0207.s1.

Corresponding author: Pengfeng Xiao, xiaopf@nju.edu.cn

DOI: 10.1175/JAMC-D-21-0207.1

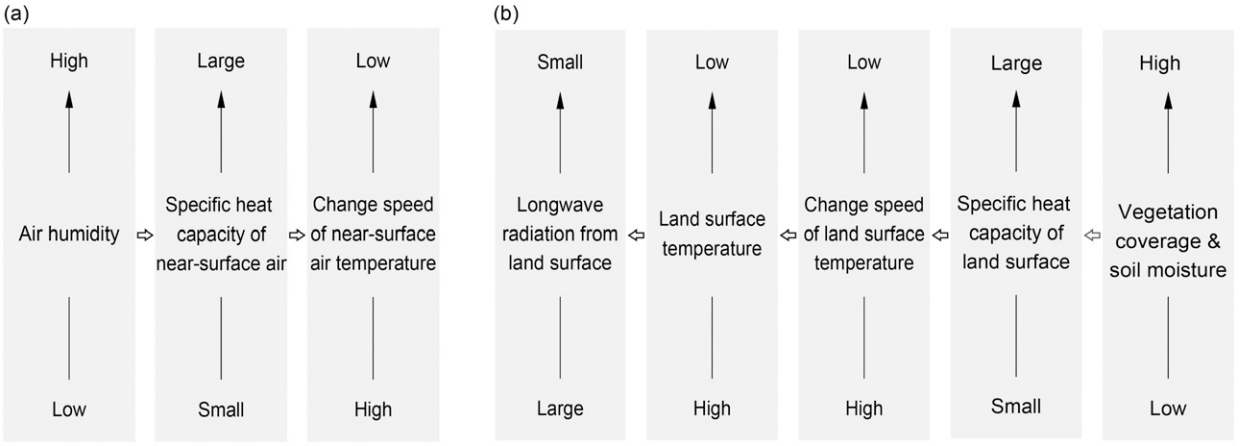

FIG. 1. (a) Mechanism showing air humidity affecting the change speed of the NSAT, and (b) vegetation coverage and soil moisture affecting longwave radiation from the land surface. The horizontal arrows represent the relationship between the left and right factors, and the vertical arrows represent the variation of each factor.

(Kattel et al. 2015; Li et al. 2013; Marshall and Losic 2011). The NSATLR is generally steeper during the day and warmer months than that during the night and colder months; namely, the steeper NSATLR occurs with stronger solar radiation (Blandford et al. 2008; Harding 1979). One explanation is that solar radiation is the major heat source indirectly affecting the rise of NSAT, and the increase in solar radiation can widen the gap of NSATs at different elevations under certain conditions, for example, when the change speed of NSAT at low elevations is larger than that at high elevations. Note that the change speed of NSAT (or land surface temperature) refers to the magnitude of the increase or decrease of NSAT (or land surface temperature) per unit of time, and its unit is degrees Celsius per second.

Air humidity has a negative relationship with NSATLR, as moist atmospheres produce weaker NSATLRs (Pepin et al. 1999). The specific heat capacity of air increases with humidity (relative humidity), and a larger specific heat capacity leads to a lower change speed of the NSAT (Fig. 1a). Therefore, an increase in air humidity can slow down the change speed of the NSAT, which is not conducive to the occurrence of large NSAT differences. The impact of synoptic conditions on NSATLR is obvious and complex, and there is often an interaction with the terrain. During synoptic-scale events, geographic differences of NSATLR are substantial, as atmospheric conditions (such as vertical structure and humidity) on the windward side are different from those on the leeward side (Minder et al. 2010). For example, when the southward cold air mass is blocked by terrain, cold air fills low-elevation regions and uplifts warm air to high-elevation regions along the windward side. Consequently, a temperature inversion will appear at the windward side, and NSATLR at the windward side will be quite different from that on the leeward side (Lundquist and Cayan 2007; Clements et al. 2003; Whiteman et al. 1999).

Although many studies have discussed the factors affecting NSATLR, there has been no study on how altitudinal differences in mountain environments (such as vegetation coverage, soil moisture, and relative humidity of near-surface air) affect NSATLRs. However, vegetation coverage and soil moisture are two key factors affecting the change speed of land surface temperature and the level of longwave radiation from the land surface (Fig. 1b). In contrast, the change speed of NSAT is negatively related to near-surface air humidity (Fig. 1a).

Furthermore, unlike the horizontal variation of NSATLR, there is limited study on the altitudinal variation of NSATLR caused by the altitudinal variations of mountain environments. In fact, the NSATLRs at different vertical belts may be obviously different due to the altitudinal variations of vegetation coverage, soil moisture, and near-surface air humidity. Thus, using the same value of NSATLR for different vertical belts may be problematic too. For instance, the mountain vertical belts in the northern slope of the Tianshan Mountains (located in a continental arid climate region) are different from those of the Alps Mountains (located in a continental humid climate region) at the same latitude. For the former, the vertical belts in ascending order of altitudes are the mountain desert belt, mountain grassland belt, mountain coniferous forest belt, alpine meadow belt, and snow–ice belt. However, the belts correspond to the broadleaved forest belt, coniferous forest belt, alpine grassland belt, alpine desert belt, and snow–ice belt for the latter. Overall, vegetation coverage, soil moisture, and near-surface air humidity on the northern slope of the Tianshan Mountains first increase and then decrease with elevation, whereas they continued to decrease with elevation in the Alps. Thus, the altitudinal variation of NSATLR on the northern slope of the Tianshan Mountains may differ from that in the Alps and other mountains.

For the Tianshan Mountains in China, existing studies on estimating NSATLR focus on five regions with different local climates (Fig. 2), including the Urumqi River basin (URB), Kaidu River basin (KRB), Yili River basin (YRB), Kunma Like River basin (KLRB), and Keqicar Baqi Glacier (KBG) (Bai 1989; Chen et al. 2013; Deng et al. 2015; Dou et al. 2011;

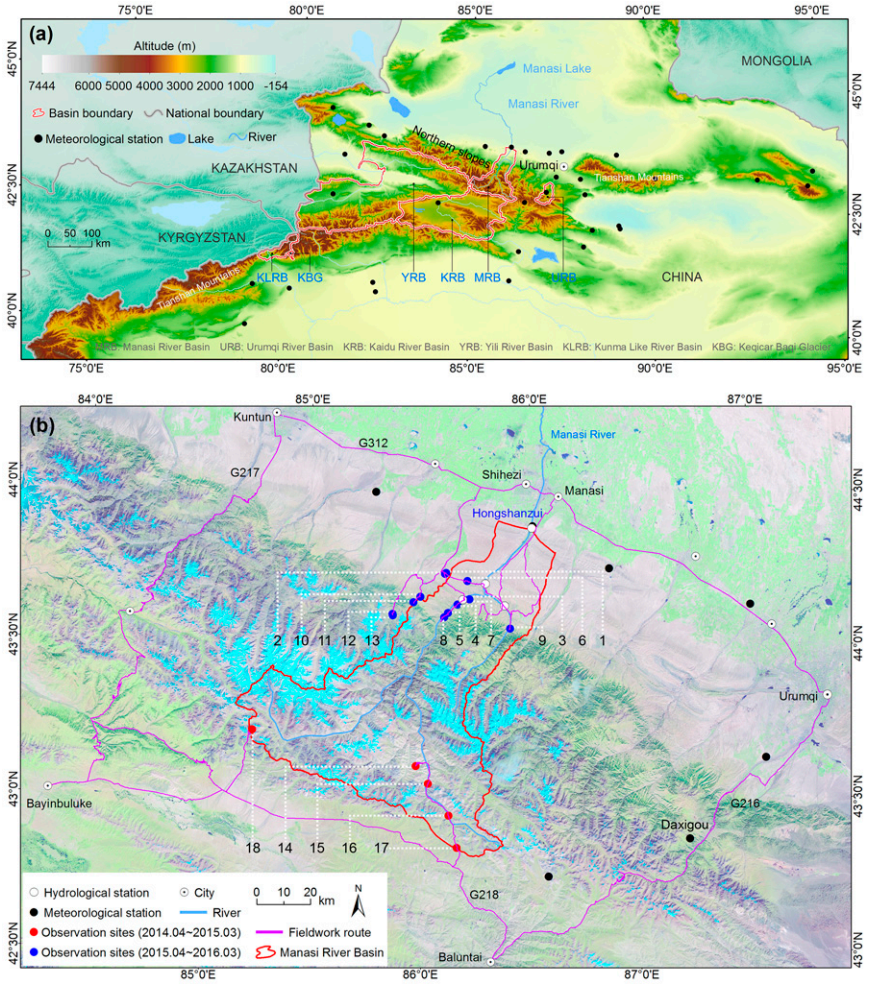

FIG. 2. (a) Location of the Manasi River basin, and (b) spatial distribution of 18 observation stations. The background of (b) is a true-color composite image of *Landsat 8* in summer, in which the light cyan represents permanent snow and ice. Labels beginning with "G" (i.e., G216, G217, G218, and G312) are national roads, numbers 1–18 are temperature stations, and white dashed lines link the number to the location.

Han et al. 2008; Wang et al. 2019; Zhang et al. 2009, 2014; Zhao et al. 2015). For the URB, the monthly NSATLRs range from −0.25° to −0.75°C per 100 m during the snowmelt period, and the largest monthly NSATLR appears in July below 2000 m but April above 2000 m (Abudu et al. 2016). For the KRB, the annual NSATLR on the south slope (−0.30°C per 100 m) is weaker than that on the north slope (−0.48°C per 100 m), and the monthly NSATLRs range from −0.65° to 0.31°C per 100 m, which steepens from January to July and weakens from July to December; besides, the positive values of the monthly NSATLRs of January, February, and December indicates that temperature inversion is existence during this period (Shen et al. 2016). For the YRB, the annual NSATLR is −0.55°C per 100 m, and the monthly NSATLRs range from −0.25°C per 100 m (January) to −0.77°C per 100 m (July) (Ye 1997). However, the NSATLR in the Manasi River basin is still unclear because of the lack of observation stations above 1000 m. A constant value (−0.6°C per 100 m) or the NSATLR in a nearby basin (Urumqi River basin) are commonly applied as a substitute in practical applications (Feng et al. 2000; Luo et al. 2013; Wang et al. 2019). However, the NSATLR in snowmelt-dominated regions varies greatly with the accumulating and melting of seasonal snow, and the local environments of these two nearby regions are not same although they are both located on the northern slope of Tianshan Mountains.

This study aims to investigate the altitudinal and temporal variations of NSATLRs in Manasi River basin on the northern slope of the Tianshan Mountains based on NSAT data from 18 observation stations, and the influence of mountain environments on the altitudinal and temporal variations of NSATLRs in the study area.

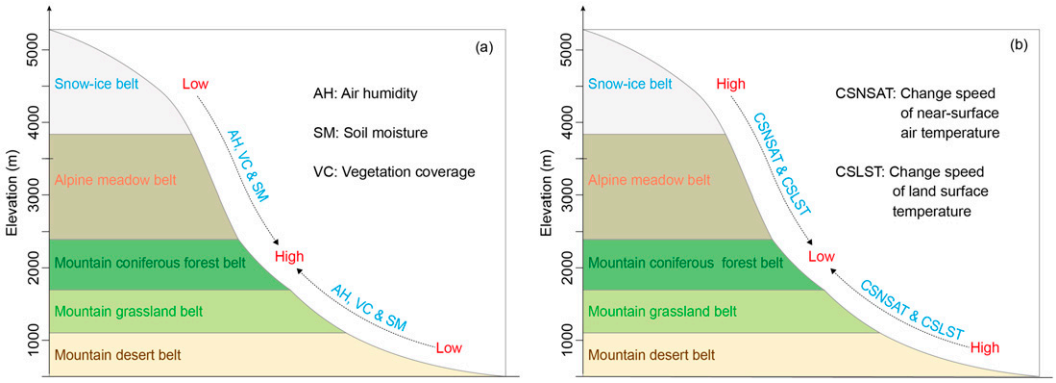

FIG. 3. (a) Altitudinal variations in local environments, and (b) the change speed of near-surface air temperature and land surface temperature in the study area.

2. Study area

The Manasi River basin is the largest snowmelt-dominated basin on the northern slope of the Tianshan Mountains (Fig. 2). The headwater of the Manasi River is situated at an elevation of ~5280 m, from which it descends to ~500 m at its outlet near the Hongshanzui hydrological station. Hundreds of glaciers and abundant seasonal snow in the mountain areas of Manasi River make it the basin with the most abundant solid water resources in this region (Hu 2004). In particular, seasonal snowmelt dominantly contributes to the spring runoff of the Manasi River, and it is a vital water resource for oasis irrigation and other purposes during spring when rainfall is low but water demand is high (Feng et al. 2018).

The mountain area of the Manasi River is divided into five vertical belts based on the altitudinal variations of landform features and vegetation types (Hu 2004), namely the mountain desert belt (400–1100 m), mountain grassland belt (1101–1600 m), mountain coniferous forest belt (1601–2400 m), alpine meadow belt (2401–3800 m), and snow–ice belt (3801–5020 m). In general, air humidity, vegetation coverage, and soil moisture increase from the mountain desert belt to mountain coniferous forest belt but decrease from mountain coniferous forest belt to snow–ice belt. Thus, change speed of NSAT and land surface temperature decrease from mountain desert belt to the mountain coniferous forest belt but increase from the mountain coniferous forest belt to the snow–ice belt, according to the reasons shown in Fig. 1. In addition, solar radiation in the study area increases from December to July but decreases from July to December (Hu 2004). The variations of land surface temperature and longwave radiation from the land surface are the same as that of solar radiation, because solar radiation is the major energy source warming the land surface, and longwave radiation from the land surface is positively correlated with land surface temperature.

The altitudinal variation of soil moisture shown in Fig. 3a is supported by the fine-resolution soil moisture data of China (Meng et al. 2021). The altitudinal variation of vegetation coverage shown in Fig. 3a is supported by the global MODIS Vegetation Continuous Fields product (DiMiceli 2017). Air humidity refers to relative humidity; in fact, there is no air humidity data that can be used to depict the elevation profile of air humidity, and the altitudinal variation of air humidity in the study area comes from our experience.

3. Data and method

a. *NSAT data*

The NSAT data were collected by 18 temperature sensors at elevations ranging from 1052 to 3920 m, covering four of the five vertical belts of the study area (Table 1). The temperature sensors were installed in solar radiation shields, and the locations of the 18 stations were relatively flat and open. Air inside and outside the solar radiation shield can circulate through the multilayer gaps of the solar radiation shield. In addition, the measured data would be more accurate if there were artificial ventilation. Figure S1 of the online supplemental material illustrates the placement and environment of the sensors for various belts. The stations in the mountain coniferous forest belt were installed at glade rather than under tree canopies. The NSAT data at 18 stations could capture the altitudinal variation of NSAT in the study area, although the spatial distribution of these stations is not optimal, as most parts of the study area are unreachable. The recording durations of the NSAT data at the 18 stations are not the same, because of the different installation dates of these temperature sensors. For stations located in the mountain grassland and mountain coniferous forest belts, the data cover April 2014–March 2015, whereas they cover April 2015–March 2016 for the alpine meadow belt and snow–ice belt. The temporal resolution of the temperature measured in the alpine meadow belt and snow–ice belt is 2 h, but it is 1 h for the mountain grassland and mountain coniferous forest belts. This is because the memory size of the sensor installed in the alpine meadow belt and snow–ice belt is not large enough for per-hour observations.

The height of the temperature sensor is approximately 30 cm above the ground, which is lower than the commonly used installation height of 2.0 m. The height of 30 cm is a compromise to accommodate available research funds and the harsh environment in the study area. In addition, according to observation

TABLE 1. Details of the 18 observation stations installed in different mountain vertical belts.

Mountain vertical belt	No.	Elev (m)	Aspect	Data recording duration
Mountain grassland belt	1	1052	Sunny slope	Apr 2015–Mar 2016
	2	1106	Shady slope	
	3	1194	Shady slope	
	4	1204	Semishady slope	
	5	1216	Semishady slope	
	6	1270	Shady slope	
	7	1350	Sunny slope	
	8	1360	Semishady slope	
	9	1450	Semishady slope	
Mountain coniferous forest belt	10	1714	Shady slope	Apr 2015–Mar 2016
	11	2100	Semisunny slope	
	12	2222	Semishady slope	
	13	2317	Shady slope	
Alpine meadow belt	14	2676	Shady slope	Apr 2014–Mar 2015
	15	2997	Semishady slope	
	16	3285	Shady slope	
	17	3550	Sunny slope	
Snow–ice belt	18	3920	Sunny slope	Apr 2014–Mar 2015

data of several years in the study area, the snow depth at the observation stations is often lower than 25 cm (Feng et al. 2018). However, temperature sensors may be snow covered when seasonal snow is thick enough. In this scenario, the measured data would be snowpack temperature instead of near-surface air temperature. Hence, these data should be removed from the estimation of NATLR to reduce error. To remove the data that were suspected to be snow covered, a conservative threshold of the daily amplitude of snowpack temperature was used in this study. In general, the daily amplitude of NSAT is greater than that of the snowpack temperature, influenced by the thermal insulation effect of snowpack. A conservative threshold (2.56°C) was supposed as the largest daily amplitude of the snowpack temperature and assumed that stations with daily amplitude above 5.0°C is not snow covered according to observation data around the study area. First, the daily amplitude of all stations was calculated based on the measured data. Second, stations with daily amplitude below the threshold and with a maximum NSAT below zero were selected as candidate stations covered by snow. Third, the candidate stations were finally labeled as snow covered if there are some nearby stations with daily amplitude above 5°C during the same day; otherwise, only the candidate stations with daily amplitude below 1°C were labeled as snow covered. Please note that it is inevitable that some stations will be mislabeled, because there is no precise threshold of the daily amplitude of snowpack temperature and there may be an intersection between the maximum-daily amplitude of the snowpack temperature and the minimum-daily amplitude of the NSAT.

b. *Estimation of NSATLR*

The hourly, daily, monthly, seasonal, and annual NSATLRs were estimated by linear regression approach. The annual, seasonal and daily NSATLRs were calculated based on the annual, seasonal, and daily average NSAT, respectively. The monthly NSATLR was computed as the mean of all daily NSATLRs for the month. First, a three-point moving average filter was applied to the original NSAT data to reduce the local noise and improve the comparability. Next, the NSATLRs were only estimated when NSAT data were simultaneously available at three or more observation stations. This criterion improves the reliability of the NSATLRs, although it reduces the number of days for which the NSATLRs can be estimated (Gardner et al. 2009).

The snow–ice belt was not considered, as the sensor installed in this belt was snow covered for most of the year, except in summer. Third, the mountain grassland and mountain coniferous forest belts were grouped into one vertical zone, and the alpine meadow belt was regarded as another vertical zone for NSATLRs estimation. As mentioned in section 2, the mountain coniferous forest belt can be regarded as an inflection point for the altitudinal variations in local environments, considering that soil moisture, vegetation coverage, and air humidity increase the from mountain desert belt to mountain coniferous forest and decrease above this belt. Thus, it is valuable to group vertical belts below the inflection point together as one vertical zone and vertical belts above the inflection point as another vertical zone, and to assess the NSATLRs of these two vertical zones.

4. Results

a. *Seasonal variation of NSATLR*

The annual NSATLR is −0.53°C per 100 m for the mountain grassland–coniferous forest belt and −0.62°C per 100 m for the alpine meadow belt. They are close to the annual NSATLR in the YRB (−0.55°C per 100 m) (Ye 1997), but larger than that in the KRB (which is −0.30°C per 100 m on the south slope and −0.48°C per 100 m on the north slopes) (Shen et al. 2016).

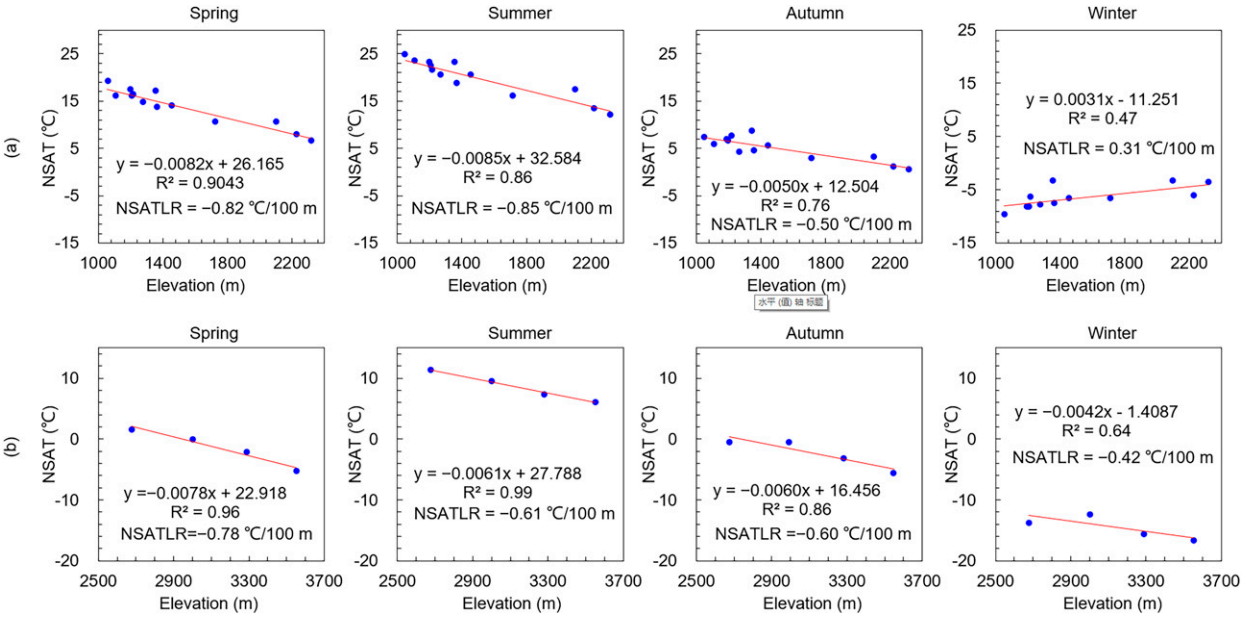

FIG. 4. Scatterplots of seasonal average NSAT data with elevation in the (top) mountain grassland–coniferous forest belt and (bottom) alpine meadow belt. Independent variable y and dependent variable x represent the seasonal average NSAT and elevation, respectively.

For the mountain grassland–coniferous forest belt, the seasonal NSATLRs range from −0.85° to 0.31°C per 100 m (Fig. 4, top panels). The positive seasonal NSATLRs during winter (December, January, and February) indicate that NSATs increase with elevation during this period, which differs from that in spring (March, April, and May), summer (June, July, and August), and autumn (September, October, and November). In addition, the annual NSATLR is weakened by the positive seasonal NSATLR in winter.

The steepest seasonal NSATLR for the mountain grassland–coniferous forest belt occurs in summer, the season with the strongest solar radiation. This phenomenon is closely related to the differences in the change speed of NSAT at different elevations, and the seasonal variation of solar radiation. A steeper NSATLR indicates a larger NSAT difference between low- and high-elevation areas, and vice versa. For the mountain grassland–coniferous forest belt, the change speed of NSAT at low-elevation areas is higher than that at high-elevation areas (Fig. 5). Meanwhile, NSAT at low-elevation areas is generally higher than that at high-elevation area in all seasons except winter. Thus, the NSAT difference between low- and high-elevation areas increases with longwave radiation in all seasons unless there is a temperature inversion (Fig. 5a; $D_2 > D_1$). Given that the strongest solar radiation in summer can cause the highest land surface temperature and longwave radiation from the land surface, the largest NSAT difference between low- and high-elevation areas will also appear in summer.

For the alpine meadow belt, annual NSATLR is −0.62°C per 100 m, and the seasonal NSATLRs range from −0.78° to −0.42°C per 100 m (Fig. 4, bottom panels). The steepest seasonal NSATLR occurs in spring (during the snowmelt period) instead of summer. This phenomenon is closely related to the altitudinal variation of seasonal snow and its high albedo and cooling effects on NSAT. The detailed reasons for this are discussed in section 4b.

b. *Monthly variation of NSATLR*

For the mountain grassland–coniferous forest belt, the monthly NSATLRs are positive from December to February (Fig. 6a). Most of the study area is affected by the cold air mass from the northwest during this period. Blocked by the terrain, the cold air mass stacks at the foot of the mountain and uplifts warm air to high-elevation areas, thus forming a stable temperature inversion layer (Hu 2004). The relatively weak value of the monthly NSATLR in November (−0.22°C per 100 m) indicates that temperature inversion may have occurred, but the temperature inversion layer is unstable and thin. The variation in the monthly NSATLR from positive value in February (0.41°C per 100 m) to negative value in March (−0.22°C per 100 m) suggested that the temperature inversion layer weakens quickly from the end of February to the beginning of March. The positive value of the monthly NSATLRs in December, January, and February (ranging from 0.32° to 0.41°C per 100 m) in this study is slightly larger than that found in KRB (ranging from 0.16° to 0.32°C per 100 m) (Shen et al. 2016), which means that temperature inversion in the study area is more obvious than that in the KRB.

The monthly NSATLRs steepen gradually from March to July, and then gradually weaken from July to November for the mountain grassland–coniferous forest belt, which is consistent with the monthly variation of solar radiation (Hu 2004; Zuo and Hou 2017). During this period, land surface temperature generally increases with increasing solar radiation and vice versa. The temporal variation of longwave radiation from

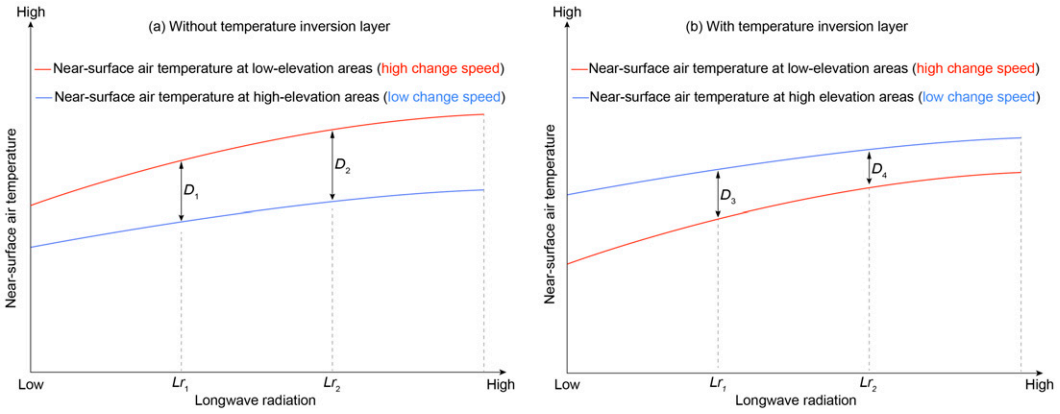

FIG. 5. Schematic diagram of the variation of NSAT in mountain grassland–coniferous forest belt if temperature inversion (a) does or (b) does not occur; Lr_1 and Lr_2 are longwave radiations at different times, and D_1, D_2, D_3, and D_4 present the absolute difference of NSATs between the low and high elevation under different situations.

the land surface is the same as that of the land surface temperature, because they are positively correlated. Meanwhile, the change speed of NSAT at low-elevation areas is higher than that at high-elevation areas. As a result, NSAT differences increase from March to July with increasing longwave radiation (Fig. 5a; $D_2 > D_1$) but decrease from July to November with decreasing longwave radiation (Fig. 5a; $D_1 < D_2$).

For the alpine meadow belt, the NSATLRs are negative during all months, ranging from −0.88°C per 100 m in April to −0.26°C per 100 m in December. The steepest monthly NSATLR occurs in April, similar to the results reported by Blandford et al. (2008) in the Rocky Mountains. Another peak of the monthly NSATLRs appears in September, that is, the beginning of the snow accumulation period.

During the snowmelt period, the monthly NSATLRs of the alpine meadow belt generally steepen from March to April and then weaken from April to June. In March and April, the impact of seasonal snow on the NSAT difference between low- and high-elevation areas is stronger than that of the other factors. This is because seasonal snow at low-elevation areas will melt and disappear first, and the snow surface temperature can be more than 20°C lower than that of nonsnow surface under the same solar radiation conditions (Feng et al. 2018). Thus, longwave radiation from the snow surface is obviously lower than that from nonsnow surface. This phenomenon will be more significant with an increase in solar radiation, as the nonsnow surface temperature increases quickly but the snow surface temperature never exceeds 0°C. Hence, NSAT differences between low-elevation areas (nonsnow surface) and high-elevation areas (snow surface) were indirectly increased by increasing solar radiation from March to April. In addition, the cooling effect of snow on NSAT further aggravates the NSAT difference between snow and nonsnow surfaces (Baker et al. 1992). However, the variation of the NSAT differences switches to a contrasting state after all seasonal snow melts from April to June. According to field observation data, seasonal snow in the alpine meadow belt disappears during early May (Feng et al. 2018). Thus, from May to June, the NSAT differences

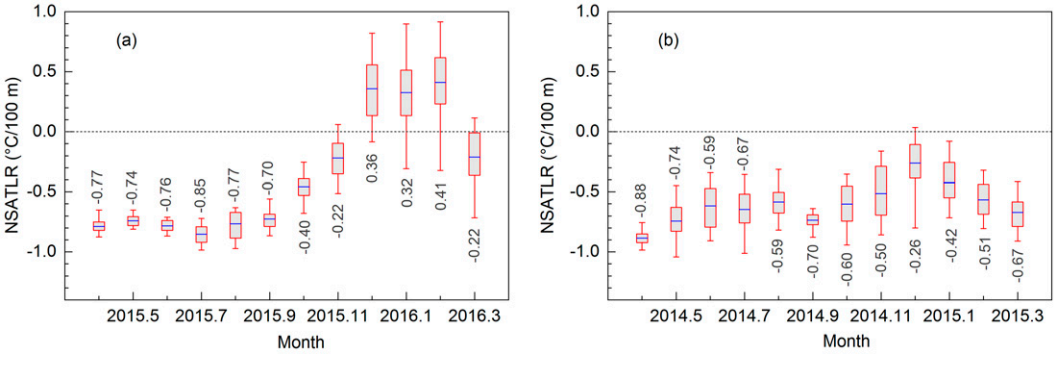

FIG. 6. Monthly variation of NSATLRs in the (a) mountain grassland–coniferous forest belt and (b) alpine meadow belt. Blue horizontal lines indicate the average of all daily NSATLRs in the month. Red boxes and whiskers show the inner quartile and full range of the daily NSATLRs, respectively. Gray numbers above or below the box are the monthly averaged NSATLRs.

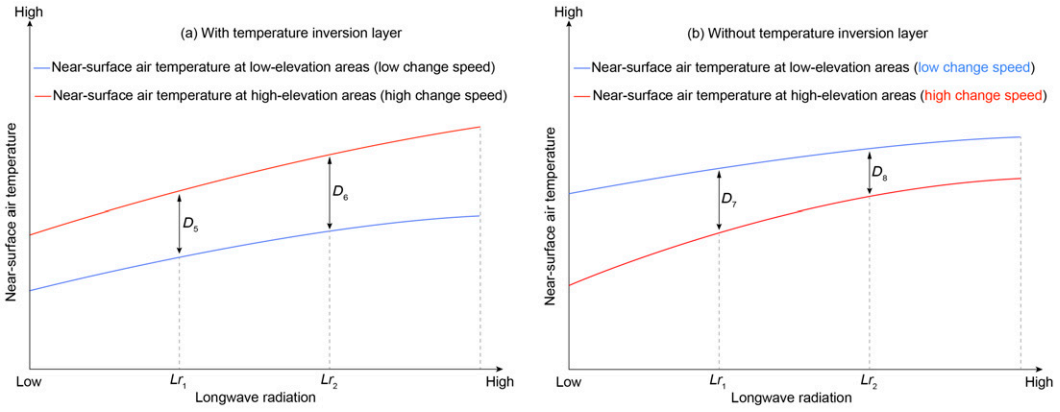

FIG. 7. As in Fig. 5, but in the alpine meadow belt.

between low and high elevations decrease with increasing longwave radiation, because the change speed of NSAT at high-elevation areas is higher than that at low-elevation areas, and NSAT at high-elevation areas is lower than that at low-elevation areas (Fig. 7b; $D_8 < D_7$).

In addition, the monthly NSATLRs from November to February could not describe accurately the altitudinal change in NSAT in the alpine meadow belt. A stable temperature inversion layer is found during this period between 2676 and 2997 m. The monthly average NSAT at 2676 m is larger than at 2997 m but lower than that at 3285 m. Therefore, the monthly NSATLRs from November to February are still negative when all the NSAT data in the alpine meadow belt were used to estimate the NSATLRs.

c. *Daily variation of NSATLR*

Only the daily variations of NSATLR on sunny days were analyzed. The daily variation of NSATLR is influenced by many random factors, especially on rainy, snowy, and cloudy days. However, on sunny days, it can be assumed that NSATLR is mainly affected by the diurnal variation of solar radiation. To obtain generalizable results on the daily variation

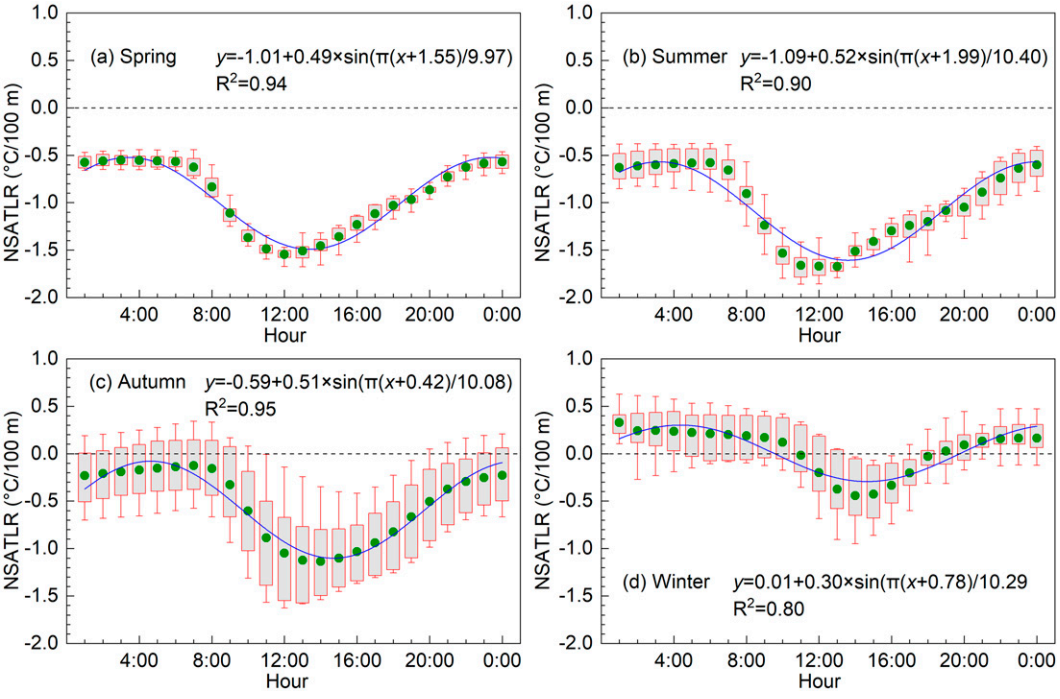

FIG. 8. Daily variation of NSATLRs on sunny days in the mountain grassland–coniferous forest belt. Blue curves present the results of the sinusoidal fit. The mathematical formula describes how the 10-day average hourly NSATLRs (y) change with time (x). Green dots indicate the average of 10-day hourly NSATLRs. Boxes and whiskers show the inner quartile and full range of the hourly NSATLR data, respectively.

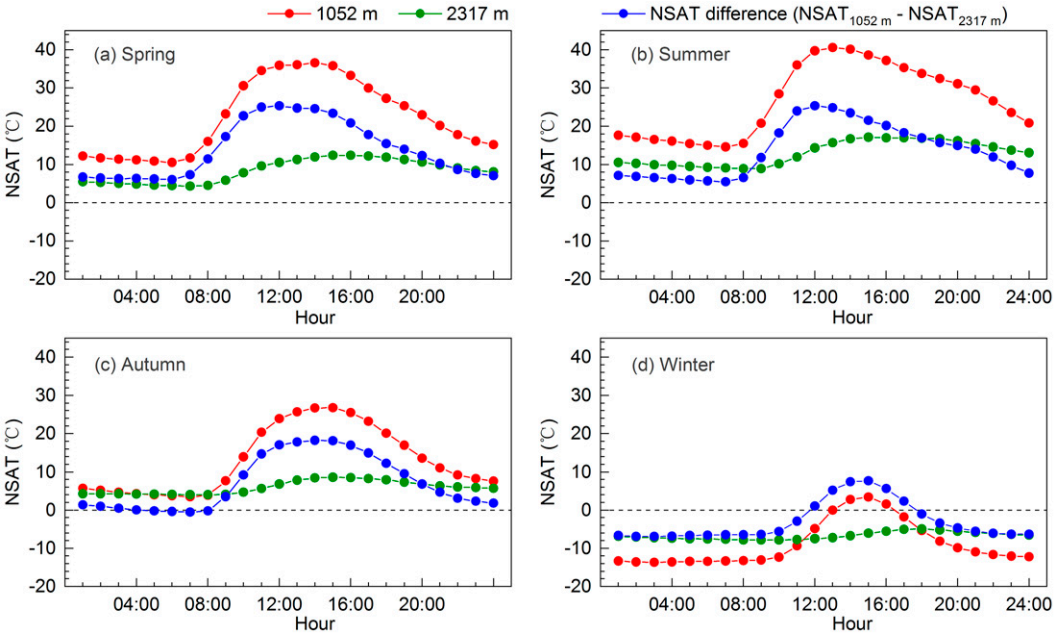

FIG. 9. Plots of 10-day average hourly NSAT data at different elevations in the mountain grassland–coniferous forest belt. Red, blue, and green lines are the connections between two adjacent dots.

of NSATLR on sunny days, NSAT data on 10 sunny days for each season were selected to calculate 10-day average hourly NSAT and 10-day average hourly NSATLRs. In addition, Beijing time referred in this section is 2 h ahead of the local time in Xinjiang, China. Sunny days were determined by checking historical weather data around the study area. Historical weather data include information such as weather conditions (sunny, cloudy, rainy, and snowy) and hourly NSAT. Moreover, the daily NSAT curve resembles a sinusoid on sunny day. Thus, only days that weather conditions in the historical weather data were sunny and daily NSAT curves resemble sinusoid were finally considered as sunny day.

For the mountain grassland–coniferous forest belt, the variation of the hourly NSATLR in spring, summer, and autumn is different from that in winter (Fig. 8). For example, the hourly NSATLRs are positive and generally steepen or weaken with increasing or decreasing NSAT, respectively, in spring, summer, and autumn. However, the hourly NSATLRs are overall positive at night but negative during the day in winter. In other words, temperature inversion at night is obvious in winter on sunny days, and it will weaken and disappear during the day. This phenomenon suggested that temperature inversion caused by southward cold air mass is not existent on sunny days during this period, and the temperature inversion at night mainly caused by cold lake effect. In spring, summer, and autumn, NSAT and its change speed at low-elevation areas are both higher than that at high-elevation areas. Thus, the NSAT difference between low- and high-elevation areas increases with increasing longwave radiation during the warming process but decreases with decreasing longwave radiation during the cooling process, as shown in Figs. 5a and 9.

In the alpine meadow belt, NSATLRs generally weaken with increasing NSAT and vice versa during spring, summer, and autumn, when the temperature inversion is absent (Fig. 10). During this period, NSAT at low-elevation areas is higher than that at high-elevation areas, while the change speed of NSAT at low-elevation areas is lower than that at high-elevation areas. Thus, the NSAT difference decreases with increasing longwave radiation and vice versa (Figs. 7b and 11). Variation of the hourly NSATLR in winter differs from those in spring, summer, and autumn. For example, temperature inversion was observed during the day, which disappears at night. In general, the NSATLR weaken with NSAT from night to day until temperature inversion occurs at 1400 Beijing time.

In general, the daily variation of the 10-day average hourly NSATLRs resembles a sinusoidal pattern. Therefore, a sine function was used to simulate the daily cycle of NSATLR on sunny days. The results show that the coefficient of determination is greater than expected, namely, the fitting of the daily cycle of the NSATLR on sunny days is effective. In addition, the coefficients of determination in winter are both the lowest for the mountain grassland–coniferous forest belt and alpine meadow belt.

5. Discussion

The lack of the NSAT data above 1000 m in the Manasi River basin has resulted in the absence of the NSATLR data for a long time. In this study, the NSATLRs of two vertical zones on seasonal, monthly, and daily scales were estimated and analyzed for the first time, combined with the altitudinal differences of mountain environments. Although the number

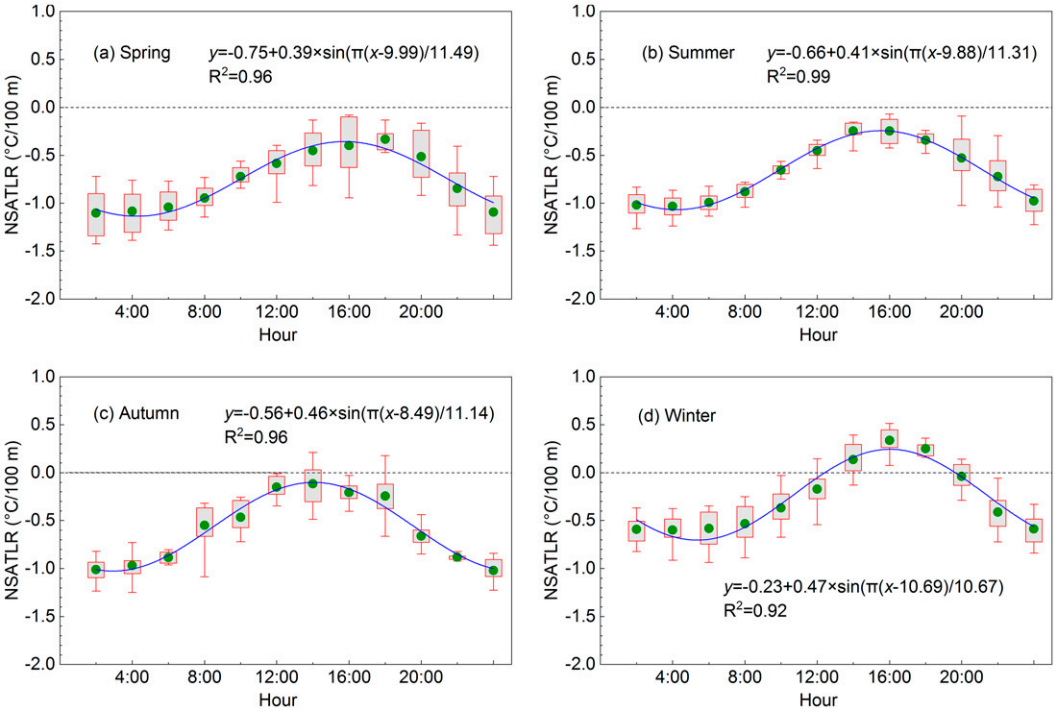

FIG. 10. As in Fig. 8, but in the alpine meadow belt.

of data are limited, these results are still valuable until alternative data become available, and the monthly NSATLRs provided in this study will benefit future studies on snowmelt runoff simulation, as the NSATLRs provided in this study are at least more accurate than a constant or the NSATLRs from other regions. Besides, there is no study revealing the impacts of vertical environment differences on the NSATLRs up to now, which is one of the major factors affecting the NSATLR. The findings of this study that the value and temporal variation (especially at monthly and daily scales) of the NSATLRs

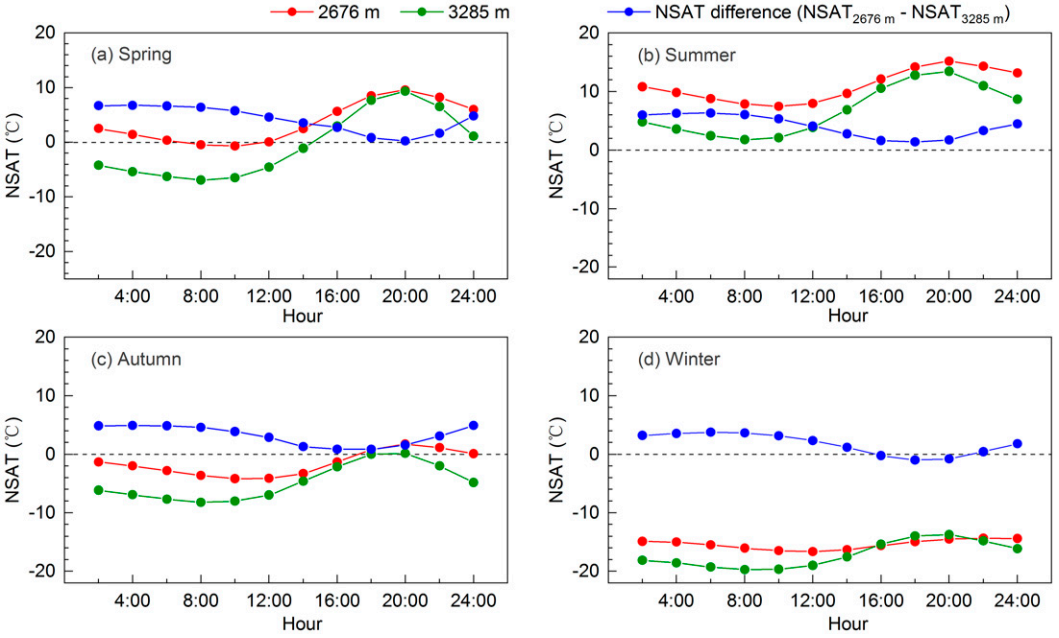

FIG. 11. As in Fig. 9, but in the alpine meadow belt.

differ greatly in different vertical zones is therefore inspiring for future study in regions with similar vertical environments. For example, the mountains with similar altitudinal environments should be divided into different vertical zones to accurately estimate the NSATLR.

However, there are five obvious limitations in this study. First, the interpretation on how the altitudinal environment differences affect the NSATLR is speculative, and the results will be more scientific if they come from simultaneous observation data (such as the outgoing longwave radiation and air humidity), although the interpretation makes sense. Second, the NSATLRs provided in this study would be more representative if the stations were evenly distributed in the study area and there were years of data available. Third, the estimation results will be more comparable if the height of the stations is the same as that of the meteorological stations. Fourth, the mislabeling of the stations (snow cover or not) is inevitable, which will influence the estimation accuracy of the NSATLR too. Therefore, more work needs to be done in the future if more data are available. Fifth, the NSAT data from different zones did not cover the same time period and thus the results might be influenced by the interannual variability.

6. Conclusions

The annual NSATLR is −0.53°C per 100 m for the mountain grassland–coniferous forest belt and −0.62°C per 100 m for the alpine meadow belt. The NSATLRs vary greatly at seasonal, monthly, and daily scales. During the snowmelt period (from March to July), the monthly NSATLRs range from −0.4° to 0.85°C per 100 m in the mountain grassland–coniferous forest belt and from −0.59° to −0.88°C per 100 m in the alpine meadow belt. The steepest monthly NSATLR occurs in July in mountain grassland–coniferous forest belt, while it occurs in April in alpine meadow belt.

The altitudinal difference of the NSATLRs between two vertical zones is obvious. The temporal variation of the NSATLRs at the mountain grassland–coniferous forest belt is different from that at the alpine meadow belt, especially at daily scale. In spring, summer, and autumn, the hourly NSATLRs in the mountain grassland–coniferous forest belt generally steepen with increasing solar radiation and weaken with decreasing solar radiation on sunny days, which is opposite to that in the alpine meadow belt. In addition, the sine function is effective for the fitting of daily variation of the hourly NSATLRs.

Acknowledgments. This work was supported by the National Natural Science Foundation of China (42001275 and 42171307), Natural Science Foundation of Hunan Province (2020JJ5980), and the Natural Science Foundation of Central South University of Forestry and Technology (2018YJ032).

Data availability statement. The near-surface air temperature data used in this study are included in the article, the vegetation coverage data used in this study are available online from the Earth data (https://doi.org/10.5067/MODIS/MOD44B.006) as cited in DiMiceli (2017), and the soil moisture data used in this study are available online from the National Science and Technology Infrastructure (https://doi.org/10.5281/zenodo.4738556) as cited in Meng et al. (2021).

REFERENCES

Abudu, S., Z. P. Sheng, C. L. Cui, M. Saydi, H.-Z. Sabzi, and J. P. King, 2016: Integration of aspect and slope in snowmelt runoff modeling in a mountain watershed. *Water Sci. Eng.*, **9**, 265–273, https://doi.org/10.1016/j.wse.2016.07.002.

Aizen, V. B., E. M. Aizen, J. M. Melack, and J. Dozier, 1997: Climatic and hydrologic changes in the Tien Shan, Central Asia. *J. Climate*, **10**, 1393–1404, https://doi.org/10.1175/1520-0442(1997)010<1393:CAHCIT>2.0.CO;2.

Bai, C. Y., 1989: A study of relationship between climate and mountain glaciers. *J. Glaciol. Geocryol.*, **11**, 287–297.

Baker, D. G., D. L. Ruschy, R. H. Skaggs, and D. B. Wall, 1992: Air temperature and radiation depressions associated with a snow cover. *J. Appl. Meteor.*, **31**, 247–254, https://doi.org/10.1175/1520-0450(1992)031<0247:ATARDA>2.0.CO;2.

Barnett, T. P., J. C. Adam, and D. P. Lettenmaier, 2005: Potential impacts of a warming climate on water availability in snow-dominated regions. *Nature*, **438**, 303–309, https://doi.org/10.1038/nature04141.

Barry, R. G., 1992: Mountain climatology and past and potential future climatic changes in mountain regions: A review. *Mt. Res. Dev.*, **12**, 71–86, https://doi.org/10.2307/3673749.

Blandford, T. R., K. S. Humes, B. J. Harshburger, B. C. Moore, V. P. Walden, and H. Ye, 2008: Seasonal and synoptic variations in near-surface air temperature lapse rates in a mountainous basin. *J. Appl. Meteor. Climatol.*, **47**, 249–261, https://doi.org/10.1175/2007JAMC1565.1.

Chen, Y., Q. Du, and Y. Chen, 2013: *Sustainable Water Use in the Bosten Lake Basin.* Science Press, 329 pp.

Clements, C. B., C. D. Whiteman, and J. D. Horel, 2003: Cold-air-pool structure and evolution in a mountain basin: Peter Sinks, Utah. *J. Appl. Meteor.*, **42**, 752–768, https://doi.org/10.1175/1520-0450(2003)042<0752:CSAEIA>2.0.CO;2.

Deng, H. J., Y. N. Chen, H. J. Wang, and S. H. Zhang, 2015: Climate change with elevation and its potential impact on water resources in the Tianshan Mountains, Central Asia. *Global Planet. Change*, **135**, 28–37, https://doi.org/10.1016/j.gloplacha.2015.09.015.

DiMiceli, M. C., 2017: MOD44B MODIS/*Terra* vegetation continuous fields yearly L3 Global 250m SIN Grid V006. NASA EOSDIS Land Processes Distributed Active Archive Center, accessed 15 May 2020, https://doi.org/10.5067/MODIS/MOD44B.006.

Dodson, R., and D. Marks, 1997: Daily air temperature interpolated at high spatial resolution over a large mountainous region. *Climate Res.*, **8**, 1–20, https://doi.org/10.3354/cr008001.

Dou, Y., X. Chen, A. M. Bao, and L. H. Li, 2011: The simulation of snowmelt runoff in the ungauged Kaidu River basin of TianShan Mountains, China. *Environ. Earth Sci.*, **62**, 1039–1045, https://doi.org/10.1007/s12665-010-0592-5.

Feng, X., W. Li, Z. Shi, and L. Wang, 2000: Satellite snow cover monitoring and Manas River snowmelt runoff simulation. *Remote Sens. Technol. Appl.*, **15**, 18–21, https://doi.org/10.3969/j.issn.1004-0323.2000.01.005.

Feng, X. Z., P. F. Xiao, X. L. Zhang, J. K. Dou, and S. P. Xie, 2018: *Remote Sensing of Snow and Its Application in Central Tianshan Mountains in China.* 1st ed. Science Press, 533 pp.

Gardner, A. S., and M. Sharp, 2017: Sensitivity of net mass-balance estimates to near-surface temperature lapse rates when employing the degree-day method to estimate glacier melt. *Ann. Glaciol.*, **50**, 80–86, https://doi.org/10.3189/172756409787769663.

——, M. J. Sharp, R. M. Koerner, C. Labine, S. Boon, S. J. Marshall, D. O. Burgess, and D. Lewis, 2009: Near-surface temperature lapse rates over Arctic glaciers and their implications for temperature downscaling. *J. Climate*, **22**, 4281–4298, https://doi.org/10.1175/2009JCLI2845.1.

Han, H. D., and Coauthors, 2008: Near-surface meteorological characteristics on the Koxkar Baxi Glacier, Tianshan. *J. Glaciol. Geocryol.*, **30**, 965–975.

Harding, R. J., 1979: Altitudinal gradients of temperature in the northern Pennines. *Weather*, **34**, 190–202, https://doi.org/10.1002/j.1477-8696.1979.tb03442.x.

Hu, R. J., 2004: *Physical Geography of the Tianshan Mountains in China*. China Environmental Science Press, 443 pp.

Immerzeel, W. W., L. P. Van Beek, and M. F. Bierkens, 2010: Climate change will affect the Asian water towers. *Science*, **328**, 1382–1385, https://doi.org/10.1126/science.1183188.

Kattel, D. B., T. Yao, W. Yang, Y. Gao, and L. Tian, 2015: Comparison of temperature lapse rates from the northern to the southern slopes of the Himalayas. *Int. J. Climatol.*, **35**, 4431–4443, https://doi.org/10.1002/joc.4297.

Li, X. P., L. Wang, D. L. Chen, K. Yang, B. L. Xue, and L. T. Sun, 2013: Near-surface air temperature lapse rates in the mainland China during 1962–2011. *J. Geophys. Res. Atmos.*, **118**, 7505–7515, https://doi.org/10.1002/jgrd.50553.

Lundquist, J. D., and D. R. Cayan, 2007: Surface temperature patterns in complex terrain: Daily variations and long-term change in the central Sierra Nevada, California. *J. Geophys. Res.*, **112**, D11124, https://doi.org/10.1029/2006JD007561.

Luo, Y., J. Arnold, S. Liu, X. Wang, and X. Chen, 2013: Inclusion of glacier processes for distributed hydrological modeling at basin scale with application to a watershed in Tianshan Mountains, northwest China. *J. Hydrol.*, **477**, 72–85, https://doi.org/10.1016/j.jhydrol.2012.11.005.

Marshall, S. J., and M. Losic, 2011: Temperature lapse rates in glacierized basins. *Encyclopedia of Snow, Ice and Glaciers*, Springer, 1145–1150.

Meng, X. J., and Coauthors, 2021: A fine-resolution soil moisture dataset for China in 2002–2018. *Earth Syst. Sci. Data*, **13**, 3239–3261, https://doi.org/10.5194/essd-13-3239-2021.

Minder, J. R., P. W. Mote, and J. D. Lundquist, 2010: Surface temperature lapse rates over complex terrain: Lessons from the Cascade Mountains. *J. Geophys. Res.*, **115**, D14122, https://doi.org/10.1029/2009JD013493.

Oerlemans, J., 2005: Extracting a climate signal from 169 glacier records. *Science*, **308**, 675–677, https://doi.org/10.1126/science.1107046.

Pepin, N., D. Benham, and K. Taylor, 1999: Modeling lapse rates in the maritime uplands of northern England: Implications for climate change. *Arct. Antarct. Alp. Res.*, **31**, 151–164, https://doi.org/10.1080/15230430.1999.12003292.

Rolland, C., 2003: Spatial and seasonal variations of air temperature lapse rates in Alpine regions. *J. Climate*, **16**, 1032–1046, https://doi.org/10.1175/1520-0442(2003)016<1032:SASVOA>2.0.CO;2.

Shen, Y. J., J. Goetz, and A. Brenning, 2016: Spatial-temporal variation of near-surface temperature lapse rates over the Tianshan Mountains, central Asia. *J. Geophys. Res. Atmos.*, **121**, 14 006–14 017, https://doi.org/10.1002/2016JD025711.

Sorg, A., T. Bolch, M. Stoffel, O. Solomina, and M. Beniston, 2012: Climate change impacts on glaciers and runoff in Tien Shan (Central Asia). *Nat. Climate Change*, **2**, 725–731, https://doi.org/10.1038/nclimate1592.

Wang, X. Y., T. Yang, C. Y. Xu, B. Yong, and P. F. Shi, 2019: Understanding the discharge regime of a glacierized alpine catchment in the Tianshan Mountains using an improved HBV-D hydrological model. *Global Planet. Change*, **172**, 211–222, https://doi.org/10.1016/j.gloplacha.2018.09.017.

Whiteman, C. D., X. Bian, and S. Zhong, 1999: Wintertime evolution of the temperature inversion in the Colorado Plateau basin. *J. Appl. Meteor.*, **38**, 1103–1117, https://doi.org/10.1175/1520-0450(1999)038<1103:WEOTTI>2.0.CO;2.

Ye, B. S., 1997: Characteristics of precipitation and temperature in the Yili River basin. *Arid Land Geogr.*, **20**, 46–52.

Zhang, F.-Y., L.-H. Li, S. Ahmad, and X.-M. Li, 2014: Using path analysis to identify the influence of climatic factors on spring peak flow dominated by snowmelt in an alpine watershed. *J. Mt. Sci.*, **11**, 990–1000, https://doi.org/10.1007/s11629-013-2789-z.

Zhang, Y., S. Liu, K. Fujita, H. Han, and J. Li, 2009: Analysis of meteorological data and the surface energy balance of Keqicar Glacier, Tien Shan, China. *Geophysical Research Abstracts*, Vol. 11, Abstract 7097, https://meetingorganizer.copernicus.org/EGU2009/EGU2009-7097-1.pdf.

Zhao, Q. D., and Coauthors, 2015: Modeling hydrologic response to climate change and shrinking glaciers in the highly glacierized Kunma Like River catchment, central Tian Shan. *J. Hydrometeor.*, **16**, 2383–2402, https://doi.org/10.1175/JHM-D-14-0231.1.

Zuo, C., and Y. Hou, 2017: Analysis on spatial-temporal variation of solar radiation in Xinjiang Region of China. *J. Anhui Agric. Sci.*, **45**, 172–178.